ACS OMEGA

Open Access

http://pubs.acs.org/journal/acsodf

Article

Aggregation-Induced Excimer Emission-Controlled Ratiometric Fluorescence Assay for Determining Critical Micelle Concentration of Surfactants

Seungyoon Kang, Gyung A Kim, and Min Su Han*

Cite This: *ACS Omega* 2025, 10, 56431−56438

Read Online

ACCESS | Metrics & More | Article Recommendations | Supporting Information

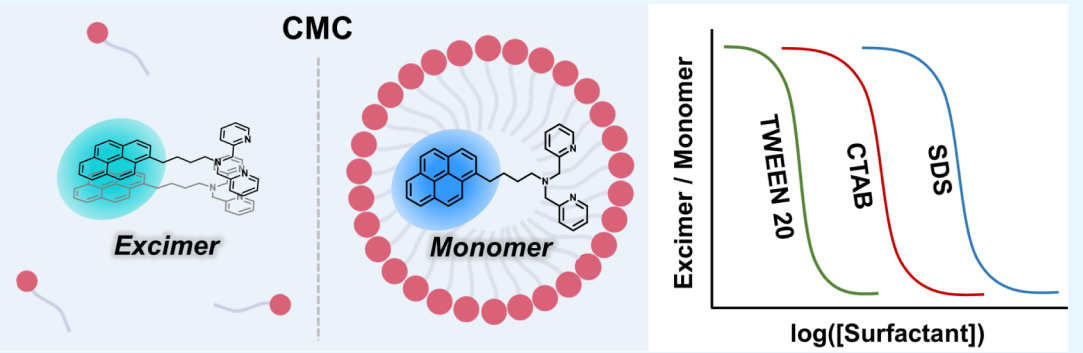

ABSTRACT: The critical micelle concentration (CMC) is a key physicochemical parameter that defines the onset of micelle formation in surfactant solutions. The determination of the CMC is essential for understanding surfactant behavior in various chemical, biological, and industrial applications. This study introduces a ratiometric fluorescence assay that exploits the distinct monomer−excimer emission behavior of pyrene-butyldipicolylamine (**Py-DPA**) to determine the CMC of various surfactants. **Py-DPA** forms self-assembled nanoaggregates in a buffered solution and exhibits strong aggregation-induced excimer emission. As the concentration of surfactant increases and micelle formation occurs, the dissolution of **Py-DPA** nanoaggregates induces a distinct fluorescence transition from excimer to monomer emission, providing a reliable indicator of micellization. The ratiometric fluorescence changes in excimer−monomer emission of **Py-DPA** enable the determination of the CMC for various surfactants, including cationic, anionic, nonionic, and zwitterionic types, demonstrating the versatility and applicability of the assay. Furthermore, the robustness and applicability of the assay are demonstrated under various conditions including variations in pH, ionic strength, and temperature.

INTRODUCTION

Surfactants are amphiphilic molecules with a crucial role in various chemical, biological, and industrial processes, including emulsification,[1] catalysis,[2−4] drug delivery,[5,6] and membrane protein stabilization.[7,8] The ability to self-assemble into micelles—spherical or other shaped aggregates formed by surfactant molecules—upon reaching or exceeding a concentration threshold known as the critical micelle concentration (CMC) is among the most fundamental properties of amphiphilic molecules. Micelle formation significantly changes the physicochemical properties of surfactants, including their solubilization capacity, surface activity, and molecular interactions in solution.[9−12] Accordingly, the determination of the CMC is essential for optimizing surfactant-based formulations and understanding their behavior in various environments.

The CMC of surfactants is traditionally determined through surface tension measurement,[13] electrical conductivity measurement,[14,15] and light scattering analysis.[16,17] In recent years, fluorescence-based assays have attracted attention as complementary techniques owing to their rapid response, ease of use, and high sensitivity.[18−20] Fluorescence-based assays have employed several fluorophores, including Nile Red,[21] coumarin derivatives,[22,23] and dansyl-based compounds,[24] to monitor changes in polarity, hydrophobicity, or microenvironment during micelle formation, providing valuable insights into micellization in several surfactant systems. Among fluorescence-based assays, those utilizing fluorophores with aggregation-induced emission (AIE) characteristics offer enhanced signals upon micelle formation, minimizing background

Received: August 19, 2025
Revised: September 25, 2025
Accepted: November 4, 2025
Published: November 10, 2025

interference and improving detection reliability.[25−29] In particular, AIE-based ratiometric fluorescence assays—which monitor the ratio between emission bands at distinct wavelengths—have emerged as effective tools owing to their intrinsic correction for environmental fluctuations, which improve the sensitivity and accuracy of CMC determination.[30,31]

Pyrene, a polycyclic aromatic hydrocarbon composed of four fused benzene rings arranged in a planar structure, serves as an effective platform for constructing ratiometric assays. Its rigid and conjugated π-system gives rise to unique photophysical properties, including strong fluorescence and the ability to form excimers under specific conditions. Excimer formation occurs when two pyrene units come into close proximity, facilitated by molecular aggregation or conformational flexibility, leading to a new emission band at a longer wavelength, distinct from monomer emission.[32,33] In particular, the structural derivatization of pyrene—through the introduction of various substituents, linkers, or functional groups—has enabled precise control over its monomer and excimer emission behavior and has been widely applied in the development of ratiometric sensors for metal ions,[34−36] anions,[37−39] and other molecular targets.[40−43] In this study, we present a ratiometric fluorescence assay for the determination of the CMC of various surfactants based on the distinct monomer−excimer emission behavior of pyrene-butyldipicolylamine (**Py-DPA**, Figure 1).

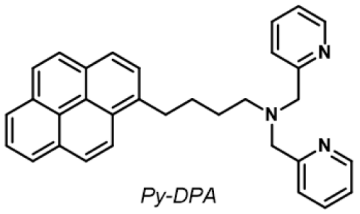

Figure 1. Structure of Py-DPA.

RESULTS AND DISCUSSION

Py-DPA exhibits an aggregation-induced excimer emission (AIEE) behavior in a buffered solution. At low concentrations, the excimer fluorescence (λ_{em} = 480 nm) of **Py-DPA** is negligible relative to its monomer fluorescence (λ_{em} = 376 nm) (Figure 2a, blue line). With increasing concentration, the monomer fluorescence of **Py-DPA** eventually saturates, whereas the excimer fluorescence significantly increases (Figure 2b). Dynamic light scattering (DLS) analysis revealed the concentration-dependent formation of **Py-DPA** nanoaggregates. In a buffered solution, 5 μM **Py-DPA** formed aggregates with a Z-average hydrodynamic diameter of 133 ± 8 nm, which increased with the **Py-DPA** concentration (Figures 2c and S1). In contrast, at **Py-DPA** concentrations below 5 μM, the scattering intensity was insufficient for reliable size determination, and the resulting data—characterized by high polydispersity and low reproducibility—suggest the absence of well-defined aggregate formation (Figure S2 and Table S1). In addition, the increased excimer fluorescence of **Py-DPA** diminished with an increase in the DMSO ratio, while the monomer fluorescence increased (Figure 2d). These observations are consistent with AIEE behavior,[30,31,44−46] indicating that **Py-DPA** forms nanoaggregates via self-assembly under the given conditions and highlighting its environmentally responsive excimer−monomer transition behavior.

Py-DPA exhibits pronounced AIEE behavior, and its excimer−monomer transition is sensitive to environmental changes. Thus, we hypothesized that this property could be effectively used for the fluorescence-based ratiometric determination of the CMC of surfactants because the **Py-DPA** nanoaggregates formed in a buffered solution are expected to dissolve upon micelle formation, thereby inducing a transition from excimer to monomer emission (Scheme 1a). To develop and validate the assay, we selected several commonly used surfactants with distinct physicochemical properties, including TWEEN 20 (a nonionic surfactant), CTAB (a cationic surfactant), SDS, SDBS (anionic surfactants), and CHAPS (a zwitterionic surfactant; Scheme 1b).

The fluorescence changes upon addition of various concentrations of the surfactant to a buffered solution containing **Py-DPA** were analyzed. The addition of low concentrations of TWEEN 20 induced a slight increase in both monomer and excimer fluorescence intensities. At concentrations near or above the CMC of TWEEN 20, the excimer emission of **Py-DPA** decreased significantly, with a corresponding increase in the monomer emission (Figure 3a). This transition reflects the disassembly of **Py-DPA** nanoaggregates upon incorporation of **Py-DPA** into micelles, demonstrating the sensitivity of the system to micelle formation. From the plot of the excimer-to-monomer fluorescence intensity ratio of **Py-DPA** as a function of the logarithm of TWEEN 20 concentration, the CMC of TWEEN 20 was determined to be 45 μM, which is in good agreement with previously reported values.[47]

To obtain mechanistic insight into the excimer-to-monomer emission transition of **Py-DPA** in response to micelle formation, ultraviolet visible (UV−vis) spectroscopy was performed. The UV−vis absorption spectrum of **Py-DPA** in DMSO exhibited three characteristic peaks at 346, 330, and 316 nm, corresponding to the vibronic transitions of the pyrene chromophore (Figure 4a, black, and Figure S3).[48] In a buffered solution, these peaks red-shifted to 353, 335, and 320 nm (Figure 4a, red), a spectral change typically associated with the formation of aggregates of organic dye compounds.[49,50] In the presence of TWEEN 20 in a buffered solution, the absorption spectrum of **Py-DPA** closely resembled that observed in DMSO (Figure 4a, blue), suggesting that **Py-DPA** was incorporated into the TWEEN 20 micelles. This interpretation was further supported by DLS analysis. In the presence of TWEEN 20 in a buffered solution, the Z-average hydrodynamic diameter of **Py-DPA** (5 μM) was measured to be 8.7 ± 0.1 nm, which is comparable to the Z-average hydrodynamic diameter of TWEEN 20 micelles (7.65 ± 0.02 nm) (Figure S4). Additional support was provided by transmission electron microscopy (TEM) and high-angle annular dark-field scanning transmission electron microscopy (HAADF-STEM). In the absence of TWEEN 20, **Py-DPA** formed irregular nanoaggregates in a buffered solution (Figure 4b). Upon addition of TWEEN 20, these nanoaggregates were no longer observed, and small, diffuse nanostructures similar in size and distribution to TWEEN 20 micelles were observed (Figures 4c,d and S5). These results suggest that **Py-DPA** aggregates were solubilized into the TWEEN 20 micelles.

The versatility of the **Py-DPA**-based ratiometric assay was further evaluated using CTAB, SDBS, SDS, and CHAPS surfactants. For all four surfactants, a similar fluorescence

https://doi.org/10.1021/acsomega.5c08403
ACS Omega 2025, 10, 56431−56438

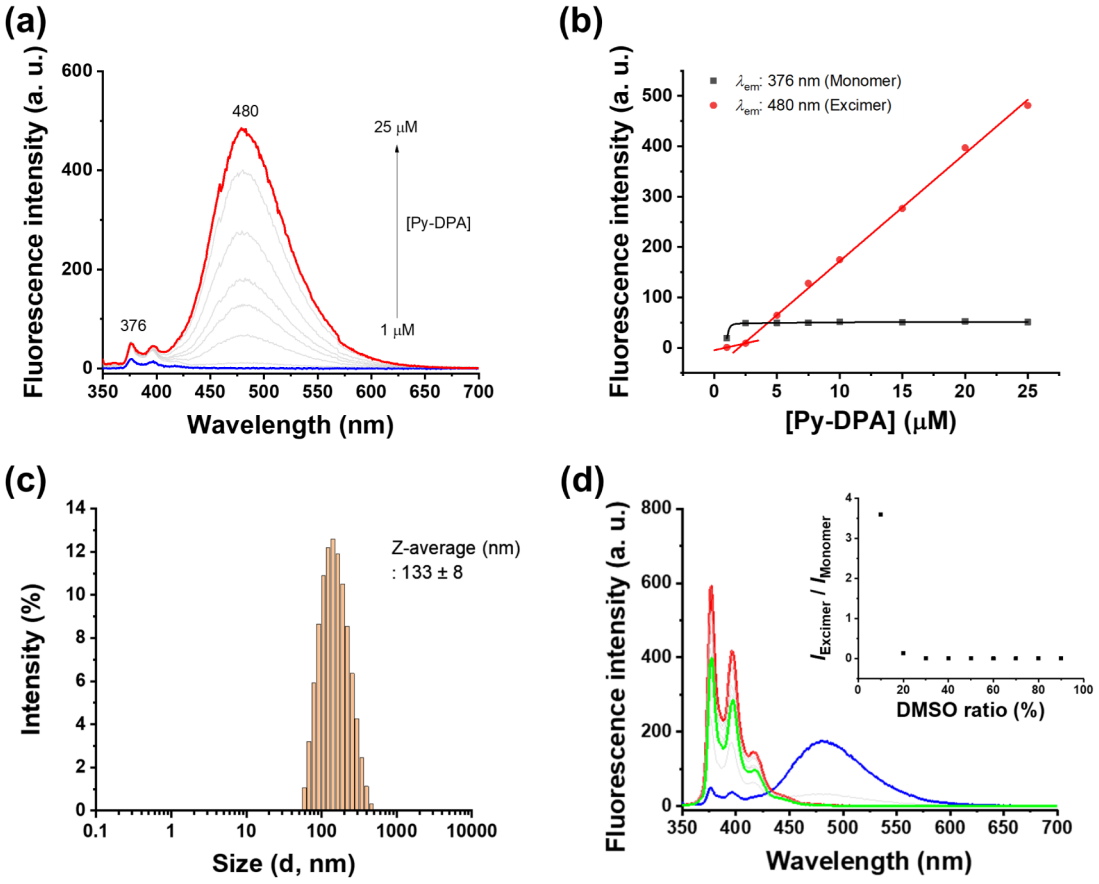

Figure 2. (a) Fluorescence spectra of various concentrations of Py-DPA in a buffered solution. Blue: 1 μM, red: 25 μM. (b) Plot of intensity of monomer (376 nm, black dot) or excimer (480 nm, red dot) fluorescence as a function of Py-DPA concentration. [Py-DPA] = 1−25 μM, [Tris−HCl] = 10 mM (pH 8.0), [EDTA] = 1 mM, 10% DMSO, λ_{ex} = 341, and λ_{em} = 350−700 nm. (c) Result of DLS analysis of Py-DPA nanoaggregates (5 μM). (d) Fluorescence spectra of Py-DPA with various DMSO ratios in a buffered solution. Blue: 10% DMSO, red: 50% DMSO, and green: 90% DMSO. Inset: Plot of fluorescence intensity ratio of excimer/monomer as a function of the DMSO ratio. [Py-DPA] = 10 μM, [Tris−HCl] = 10 mM (pH 8.0), [EDTA] = 1 mM, DMSO ratio = 10−90% (v/v), λ_{ex} = 341, and λ_{em} = 350−700 nm.

transition pattern was observed near their respective CMCs, characterized by a sharp decrease in excimer emission and a corresponding increase in monomer emission (Figures 5 and S6−S9). This consistent behavior enabled an accurate determination of the CMC values for each surfactant. Specifically, the CMCs of CTAB, SDBS, SDS, and CHAPS were determined to be 0.278 mM, 0.65 mM, 2.20 mM, and 3.799 mM, respectively, which are in good agreement with previously reported values (Table 1). These findings demonstrate that the **Py-DPA**-based ratiometric fluorescence assay is broadly applicable for determining the CMCs of various surfactants with differing ionic properties.

Furthermore, the robustness and applicability of the **Py-DPA**-based ratiometric assay were evaluated under various conditions, including variations in pH, ionic strength, and temperature. To investigate the influence of pH and buffer systems, the CMC of TWEEN 20 was determined by using the **Py-DPA**-based ratiometric assay in three different buffers: MES (pH 5.5), HEPES (pH 7.4), and CHES (pH 9.5). At pH 7.4 and 9.5, fluorescence transition patterns similar to those observed at pH 8.0 were observed, allowing the CMCs to be determined as 50 and 44 μM, respectively (Figures S10 and S11). Interestingly, at pH 5.5, the excimer fluorescence of **Py-DPA** was relatively low, which may be attributed to the solubility change of **Py-DPA** caused by protonation of the pyridine moiety. Nevertheless, upon addition of TWEEN 20, excimer fluorescence slightly increased, and near the CMC, a characteristic decrease in excimer fluorescence was observed. This change enabled ratiometric analysis, allowing the CMC to be determined as 45 μM at pH 5.5 (Figure S12).

To investigate the influence of ionic strength, the CMC of SDS was determined using the **Py-DPA**-based ratiometric assay in the presence of varying concentrations of NaCl (100, 250, and 500 mM). As the salt concentration increased, the CMC of SDS gradually decreased, with values determined to be 1.81 mM, 1.04 mM, and 0.68 mM, respectively (Figures 6 and S13−S15), which is consistent with previously reported trends.[53,54] In addition, the effect of the temperature on micelle formation was examined by performing the assay after incubation at 60 °C. A clear fluorescence transition was still observed, and the CMC of SDS at 60 °C was determined to be 6.1 mM (Figure S16).[53,55] These results indicate that the **Py-DPA**-based ratiometric assay can reliably reflect and quantify changes in the CMC of surfactants under diverse environmental conditions.

CONCLUSIONS

A ratiometric fluorescence assay based on the AIEE behavior of **Py-DPA** was developed to determine the CMC of various surfactants. **Py-DPA** forms self-assembled nanoaggregates in a buffered solution and exhibits strong AIEE. The nano-

https://doi.org/10.1021/acsomega.5c08403
ACS Omega 2025, 10, 56431−56438

Scheme 1. (a) Schematic of Py-DPA-Based Determination of CMC of Surfactants; (b) Structure of Surfactants

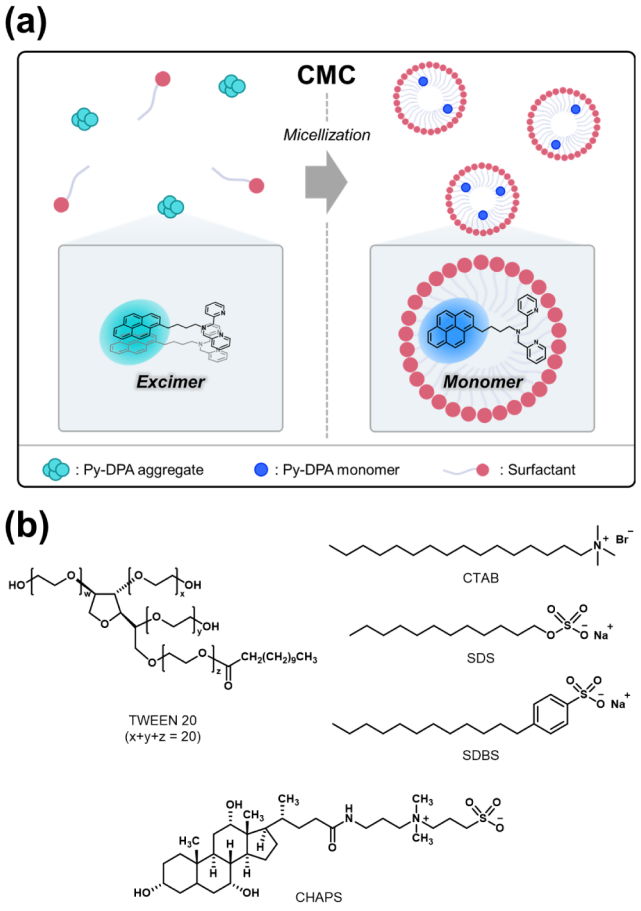

aggregates of **Py-DPA** exhibited a distinct and reproducible excimer-to-monomer emission transition upon disassembly induced by micelle formation, enabling determination of the CMC. The assay allowed the successful determination of the CMCs of various surfactants with different ionic properties, including nonionic, cationic, anionic, and zwitterionic surfactants; the measured CMC values showed good agreement with previously reported values. Furthermore, the assay demonstrated reliable performance under a range of environmental conditions, including variations in pH, ionic strength, and temperature. The results demonstrate the broad applicability and reliability of the **Py-DPA**-based ratiometric fluorescence assay as a convenient and effective tool for determining the CMC of surfactants.

EXPERIMENTAL SECTION

Materials and Instruments. Chemical reagents were purchased from commercial sources (Sigma-Aldrich, Alfa Aesar, Tokyo Chemical Industry, Duksan Pure Chemicals, and Daejung Chemicals), unless otherwise stated, and used without further purification. All surfactants used in this study were purchased from Sigma-Aldrich and used without further purification, including TWEEN 20 (Cat. No. P1379), cetyltrimethylammonium bromide (CTAB, Cat. No. H6269), sodium dodecylbenzenesulfonate (SDBS, Cat. No. 289957), sodium dodecyl sulfate (SDS, Cat. No. L4509), and 3-[(3-cholamidopropyl)dimethylammonio]-1-propanesulfonate (CHAPS, Cat. No. 10810118001). A 100× Tris−EDTA buffer

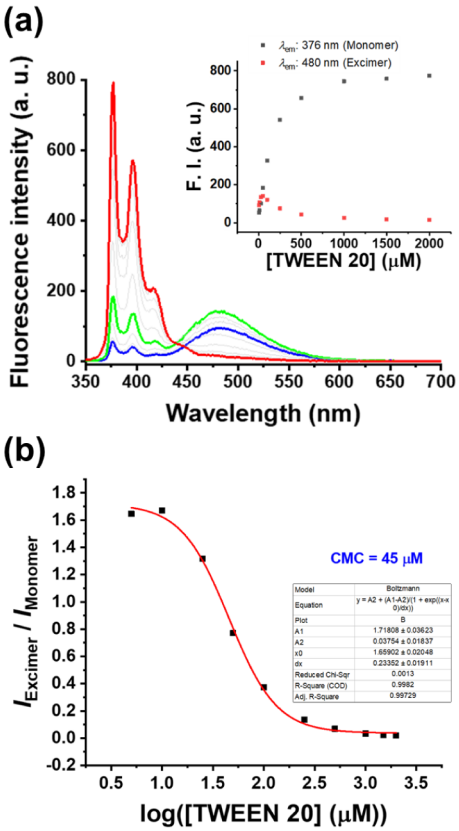

Figure 3. (a) Fluorescence spectra of Py-DPA in the presence of various concentrations of TWEEN 20. Blue: 5 μM, green: 50 μM, red: 2000 μM. Inset: Plot of intensity of monomer (376 nm, black dot) or excimer (480 nm, red dot) fluorescence as a function of TWEEN 20 concentration. [Py-DPA] = 5 μM, [Tris−HCl] = 10 mM (pH 8.0), [EDTA] = 1 mM, 10% DMSO, λ_{ex} = 341, and λ_{em} = 350−700 nm. (b) Plot of fluorescence intensity ratio of excimer-to-monomer of Py-DPA as a function of logarithm of concentration of TWEEN 20.

(pH 8.0) was obtained from Sigma-Aldrich and appropriately diluted with distilled water prior to use. Other buffer solutions (pH 5.5 MES, pH 7.4 HEPES, and pH 9.5 CHES) were prepared in-house.

NMR spectra were recorded on a JEOL 400 MHz NMR spectrometer. Fluorescence spectra were recorded using an Agilent Cary Eclipse fluorescence spectrometer with a semimicro quartz cuvette (Hellma, Cat. No. 114F-QS). UV−vis spectra were obtained using an Agilent Cary 8454 UV−vis spectrophotometer with a semimicro quartz cuvette (Hellma, Cat. No. 114B-QS). DLS analyses were performed using a Malvern Instruments Zetasizer Nano ZSP. TEM and HAADF-STEM analyses were conducted on a Tecnai G2 F30 S-Twin (300 keV, FEI) using carbon-coated 400-mesh copper grids (Electron Microscopy Sciences, Cat. No. CF400-Cu-50-UL). Temperature-controlled experiments were conducted by using a heating shaker (Jeio Tech, CBS-350). pH measurements were performed by using a pH meter (Mettler Toledo, SevenCompact S210) in combination with a pH electrode (Mettler Toledo, InLab Routine Pro-ISM).

Synthesis of Py-DPA. **Py-DPA** was synthesized according to a previously reported method, and the obtained ^{1}H and ^{13}C NMR data showed good agreement with the previously reported values.[56−59] ^{1}H NMR (400 MHz, $CDCl_3$) δ 8.50 (d, J = 4.1 Hz, 2H), 8.15−8.23 (m, 3H), 7.97−8.09 (m, 5H), 7.79

https://doi.org/10.1021/acsomega.5c08403
ACS Omega 2025, 10, 56431−56438

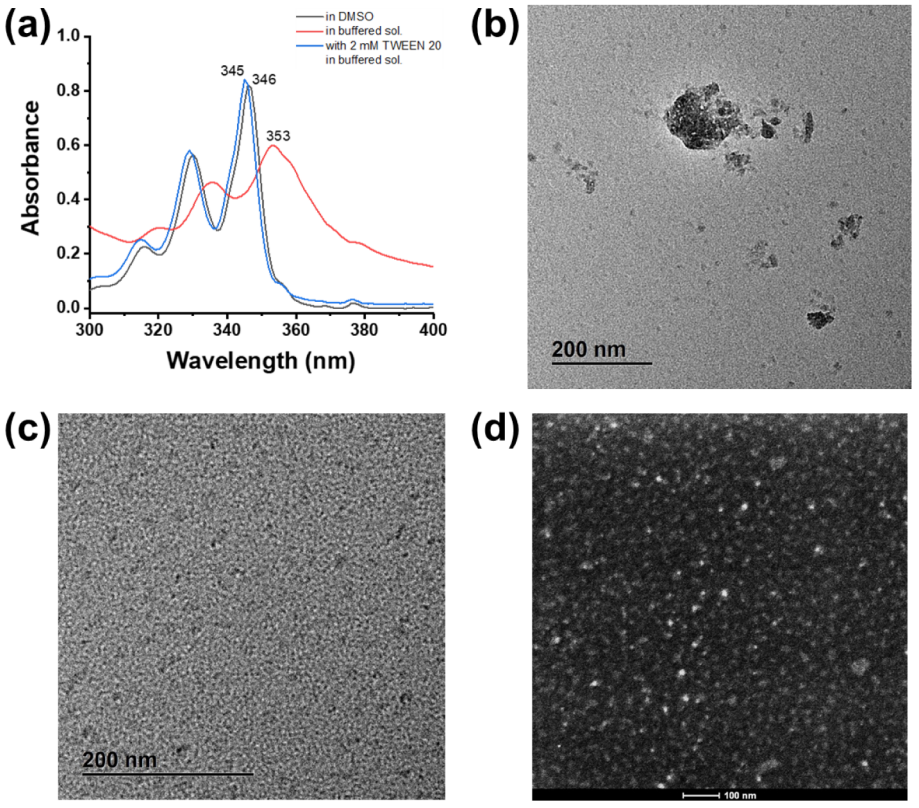

Figure 4. (a) UV−vis spectra of Py-DPA (25 μM) in DMSO (black), in a buffered solution in the absence of TWEEN 20 (red), and in the presence of 2 mM TWEEN 20 (blue). Buffer conditions: [Tris−HCl] = 10 mM (pH 8.0), [EDTA] = 1 mM, and 10% DMSO. (b) TEM image of Py-DPA nanoaggregates. (c, d) TEM and HAADF-STEM images of Py-DPA in the presence of TWEEN 20.

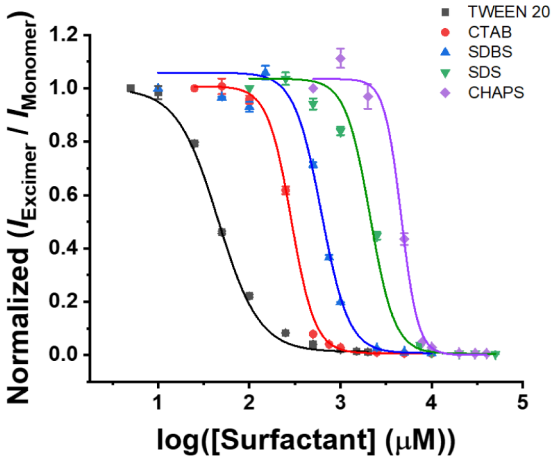

Figure 5. Plot of normalized fluorescence ratio of excimer-to-monomer of Py-DPA as a function of the logarithm of concentration of surfactants. Black: TWEEN 20, red: CTAB, blue: SDBS, green: SDS, and purple: CHAPS.

Table 1. Summary of CMC Value of Surfactants

Surfactant	Calculated CMC[a,b]	Reported CMC
TWEEN 20	0.045 ± 0.001 mM	0.05 mM[c]
CTAB	0.278 ± 0.006 mM	0.2 mM[d]
SDBS	0.65 ± 0.02 mM	0.61 mM[e]
SDS	2.20 ± 0.08 mM	1.99 mM[d]
CHAPS	3.799 ± 0.001 mM	4.0 mM[f]

[a]Obtained from fluorescence assay using a Py-DPA. [b]Values represent the mean ± standard deviation from three independent experiments with freshly prepared samples. [c]In water.[47] [d]pH 7.0, phosphate buffer.[11,51] [e]pH 6.8, phosphate buffer.[17] [f]pH 7.4, HEPES buffer.[52]

(d, J = 7.8 Hz, 1H), 7.56 (td, J = 7.8, 1.8 Hz, 2H), 7.47 (d, J = 7.8 Hz, 2H), 7.08−7.11 (m, 2H), 3.81 (s, 4H), 3.27 (t, J = 7.8 Hz, 2H), 2.64 (t, J = 7.3 Hz, 2H), 1.81−1.89 (m, 2H), 1.68−1.75 (m, 2H). ^{13}C NMR (100 MHz, $CDCl_3$) δ 160.08, 148.99, 136.97, 136.42, 131.52, 130.99, 129.80, 128.66, 127.61, 127.30, 127.18, 126.61, 125.86, 125.15, 125.12, 124.89, 124.84, 124.72, 123.57, 122.95, 121.94, 60.68, 54.41, 33.39, 29.49, 27.25.

Concentration-Dependent Fluorescence Analysis of Py-DPA. Various concentrations of **Py-DPA** (10−250 μM in DMSO, 100 μL) were added to 900 μL of Tris-EDTA buffer (pH 8.0) solution. After vortexing for 3 s, the resulting mixtures (total volume: 1000 μL) were transferred to a quartz cuvette, and fluorescence spectra were recorded. The final concentrations were as follows: [**Py-DPA**] = 1−25 μM, DMSO content = 10% (v/v), [Tris-HCl] = 10 mM, and [EDTA] = 1 mM.

Fluorescence Behavior of Py-DPA in Response to DMSO Content. A mixture of DMSO and Tris-EDTA buffer solution (pH 8.0) with varying volume ratios (DMSO/water = 0/9 to 8/1, v/v; total volume: 900 μL) was prepared, to which **Py-DPA** (100 μM in DMSO, 100 μL) was added. After vortexing for 3 s, the resulting mixtures (final volume: 1000 μL) were transferred to a quartz cuvette, and fluorescence spectra were recorded. The final concentrations were: [**Py-DPA**] = 10 μM, DMSO content = 10−90% (v/v), [Tris-HCl] = 10 mM, and [EDTA] = 1 mM.

DLS Analysis of Py-DPA Nanoaggregates and TWEEN 20 Micelles. *Py-DPA Nanoaggregates.* Various concentra-

https://doi.org/10.1021/acsomega.5c08403
ACS Omega 2025, 10, 56431−56438

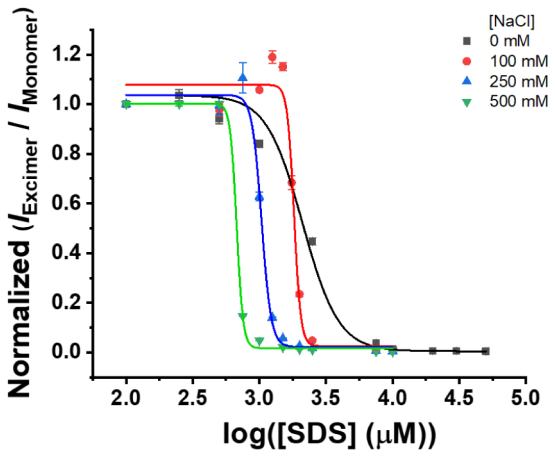

Figure 6. Plot of normalized fluorescence ratio of excimer-to-monomer of Py-DPA as a function of logarithm of concentration of SDS under varying concentrations of NaCl: black, 0 mM, red: 100 mM, blue: 250 mM, and green: 500 mM.

tions of **Py-DPA** (10−250 μM in DMSO, 100 μL) were added to 900 μL of Tris-EDTA buffer solution (pH 8.0). After vortexing for 3 s, the resulting mixtures (final volume: 1000 μL) were transferred to a quartz cuvette for DLS analysis. Each sample was measured three times after a 120-s equilibration period, using automatically optimized run counts and attenuator settings. The Z-average hydrodynamic diameter of **Py-DPA** nanoaggregates was determined from the intensity-based size distribution report. The final concentrations were as follows: [**Py-DPA**] = 1−25 μM, DMSO content = 10% (v/v), [Tris-HCl] = 10 mM, and [EDTA] = 1 mM. Dispersant parameters were set as follows: viscosity = 1.0 cP, refractive index = 1.348, and dielectric constant = 74.

TWEEN 20 Micelles. TWEEN 20 (10 mM in water, 200 μL) was added to the mixture of Tris-EDTA buffer (pH 8.0) and DMSO (buffer/DMSO = 8/1, v/v; total volume: 800 μL). After vortexing for 3 s, the resulting mixture (final volume: 1000 μL) was transferred to a quartz cuvette, and DLS analysis was performed. The final concentrations were as follows: [TWEEN 20] = 2 mM, DMSO content = 10% (v/v), [Tris-HCl] = 10 mM, and [EDTA] = 1 mM.

Py-DPA in the Presence of TWEEN 20 Micelles. **Py-DPA** (50 μM in DMSO, 100 μL) was added to 900 μL of a Tris-EDTA buffer solution (pH 8.0) containing TWEEN 20. After vortexing for 3 s, the resulting mixture (final volume: 1000 μL) was transferred to a quartz cuvette, and DLS analysis was performed. The final concentrations were as follows: [**Py-DPA**] = 5 μM, [TWEEN 20] = 2 mM, DMSO content = 10% (v/v), [Tris-HCl] = 10 mM, and [EDTA] = 1 mM.

Determination of the CMC of Surfactants Using Py-DPA. Various concentrations of TWEEN 20 (50−20,000 μM in water, 100 μL) were added to 900 μL of Tris-EDTA buffer solution (pH 8.0) containing **Py-DPA** dissolved in DMSO. After vortexing for 3 s, the resulting mixtures (final volume: 1000 μL) were transferred to a quartz cuvette, and fluorescence spectra were recorded. The CMC was determined by fitting the plot of log ([TWEEN 20]) as a function of the excimer-to-monomer fluorescence intensity ratio using a Boltzmann function, where the inflection point (x_0) was used as the CMC value. All experiments were performed three times independently, and the results were averaged. Similar procedures were applied to other surfactants using appropriate concentration ranges. The final concentrations were as follows: [**Py-DPA**] = 5 μM, [TWEEN 20] = 5−2000 μM, DMSO content = 10% (v/v), [Tris-HCl] = 10 mM, and [EDTA] = 1 mM.

Evaluation of Robustness and Applicability of the Py-DPA-Based Ratiometric Assay. *Effect of pH.* **Py-DPA** (50 μM in DMSO, 100 μL) was added to 900 μL of buffer solution (pH 5.5 MES, pH 7.4 HEPES, or pH 9.5 CHES) containing various concentrations of TWEEN 20. After vortexing for 3 s, the resulting mixtures (final volume: 1000 μL) were transferred to a quartz cuvette, and fluorescence spectra were recorded. The CMC was determined by fitting the plot of log([TWEEN 20]) as a function of the excimer-to-monomer fluorescence intensity ratio using a Boltzmann function, where the inflection point (x_0) was used as the CMC value. For pH 5.5, the data were fitted using a Voigt function, and the center position (x_c) was used to determine the CMC value. The final concentrations were as follows: [**Py-DPA**] = 5 μM, [TWEEN 20] = 5−2000 μM, [Buffers] = 10 mM, and DMSO content = 10% (v/v).

Effect of Ionic Strength. **Py-DPA** (50 μM in DMSO, 100 μL) was added to 900 μL of a Tris-EDTA buffer solution (pH 8.0) containing various concentrations of SDS and NaCl. After vortexing for 3 s, the resulting mixtures (final volume: 1000 μL) were transferred to a quartz cuvette, and fluorescence spectra were recorded. The CMC was determined by fitting the plot of log([SDS]) as a function of the excimer-to-monomer fluorescence intensity ratio using a Boltzmann function, where the inflection point (x_0) was used as the CMC value. The final concentrations were as follows: [**Py-DPA**] = 5 μM, [SDS] = 100−10000 μM, [NaCl] = 0, 100, 250, or 500 mM, [Tris-HCl] = 10 mM, [EDTA] = 1 mM, and DMSO content = 10% (v/v).

Effect of Temperature. A total of 900 μL of Tris-EDTA buffer (pH 8.0) containing various concentrations of SDS was incubated in a heating shaker at 60 °C with shaking (800 rpm) for 5 min. **Py-DPA** (50 μM in DMSO, 100 μL) was then added to the mixtures, which were vortexed for 3 s, transferred quickly to a quartz cuvette, and subjected to fluorescence spectral analysis. The CMC was determined by fitting the plot of log([SDS]) as a function of the excimer-to-monomer fluorescence intensity ratio using a Boltzmann function, where the inflection point (x_0) was used as the CMC value. The final concentrations were as follows: [**Py-DPA**] = 5 μM, [SDS] = 100−30000 μM, [Tris-HCl] = 10 mM, [EDTA] = 1 mM, and DMSO content = 10% (v/v).

■ ASSOCIATED CONTENT

Supporting Information

The Supporting Information is available free of charge at https://pubs.acs.org/doi/10.1021/acsomega.5c08403.

Result of DLS analysis; TEM analysis; UV−vis spectra; fluorescence spectra; CMC determination; NMR spectra of **Py-DPA** (PDF)

■ AUTHOR INFORMATION

Corresponding Author

Min Su Han − *Department of Chemistry, Gwangju Institute of Science and Technology (GIST), Gwangju 61005, Republic of Korea;* orcid.org/0000-0001-9588-6980; Email: happyhan@gist.ac.kr

https://doi.org/10.1021/acsomega.5c08403
ACS Omega 2025, 10, 56431−56438

Authors

Seungyoon Kang − *Department of Chemistry, Gwangju Institute of Science and Technology (GIST), Gwangju 61005, Republic of Korea*

Gyung A Kim − *Department of Chemistry, Gwangju Institute of Science and Technology (GIST), Gwangju 61005, Republic of Korea*

Complete contact information is available at: https://pubs.acs.org/10.1021/acsomega.5c08403

Notes

The authors declare no competing financial interest.

■ ACKNOWLEDGMENTS

This work was supported by the National Research Foundation of Korea (NRF) grant funded by the Korea government (MSIT) (RS-2023-00220174).

■ REFERENCES

(1) Li, L.; Su, Q.; Xu, K.; Ren, L.; Zhao, Q.; Wu, Q.; Xia, J.; Lü, X.; Wang, L. Self-Assembly of Cinnamic Acid-Modified Chitosan Surfactants: Synthesis, Characterization, and Applications in Emulsification. *ACS Sustainable Chem. Eng.* **2024**, *12*, 7541−7552.

(2) Qu, R.; Shen, L.; Chai, Z.; Jing, C.; Zhang, Y.; An, Y.; Shi, L. Hemin-Block Copolymer Micelle as an Artificial Peroxidase and Its Applications in Chromogenic Detection and Biocatalysis. *ACS Appl. Mater. Interfaces* **2014**, *6*, 19207−19216.

(3) Wang, C.; Hong, H.; Chen, M.; Ding, Z.; Rui, Y.; Qi, J.; Li, Z.-C.; Liu, Z. A Cationic Micelle as In Vivo Catalyst for Tumor Localized Cleavage Chemistry. *Angew. Chem., Int. Ed.* **2021**, *60*, 19750−19758.

(4) Sharma, B.; Striegler, S. Polarity and Critical Micelle Concentration of Surfactants Support the Catalytic Efficiency of Nanogels during Glycoside Hydrolyses. *ACS Catal.* **2022**, *12*, 8841−8847.

(5) Lu, Y.; Yue, Z.; Xie, J.; Wang, W.; Zhu, H.; Zhang, E.; Cao, Z. Micelles with ultralow critical micelle concentration as carriers for drug delivery. *Nat. Biomed. Eng.* **2018**, *2*, 318−325.

(6) Xiang, J.; Shen, Y.; Zhang, Y.; Liu, X.; Zhou, Q.; Zhou, Z.; Tang, J.; Shao, S.; Shen, Y. Multipotent Poly(Tertiary Amine-Oxide) Micelles for Efficient Cancer Drug Delivery. *Adv. Sci.* **2022**, *9* (12), 2200173.

(7) Frotscher, E.; Danielczak, B.; Vargas, C.; Meister, A.; Durand, G.; Keller, S. A Fluorinated Detergent for Membrane-Protein Applications. *Angew. Chem., Int. Ed.* **2015**, *54*, 5069−5073.

(8) Wehbie, M.; Onyia, K. K.; Mahler, F.; Le Roy, A.; Deletraz, A.; Bouchemal, I.; Vargas, C.; Babalola, J. O.; Breyton, C.; Ebel, C.; Keller, S.; Durand, G. Maltose-Based Fluorinated Surfactants for Membrane-Protein Extraction and Stabilization. *Langmuir* **2021**, *37*, 2111−2122.

(9) Wennerström, H.; Lindman, B. Micelles. Physical chemistry of surfactant association. *Phys. Rep.* **1979**, *52* (1), 1−86.

(10) Lamont, R. E.; Ducker, W. A. Surface-Induced Transformations for Surfactant Aggregates. *J. Am. Chem. Soc.* **1998**, *120*, 7602−7607.

(11) Fuguet, E.; Ràfols, C.; Rosés, M.; Bosch, E. Critical micelle concentration of surfactants in aqueous buffered and unbuffered systems. *Anal. Chim. Acta* **2005**, *548*, 95−100.

(12) Cui, X.; Mao, S.; Liu, M.; Yuan, H.; Du, Y. Mechanism of Surfactant Micelle Formation. *Langmuir* **2008**, *24* (19), 10771−10775.

(13) Nyuta, K.; Yoshimura, T.; Esumi, K. Surface tension and micellization properties of heterogemini surfactants containing quaternary ammonium salt and sulfobetaine moiety. *J. Colloid Interface Sci.* **2006**, *301*, 267−273.

(14) Chang, H.-C.; Lin, Y.-Y.; Chern, C.-S.; Lin, S.-Y. Determination of Critical Micelle Concentration of Macroemulsions and Miniemulsions. *Langmuir* **1998**, *14*, 6632−6638.

(15) Goronja, J.; Pejić, N.; Janošević Ležaić, A.; Stanisavljev, D.; Malenović, A. Using a Combination of Experimental and Mathematical Method To Explore Critical Micelle Concentration of a Cationic Surfactant. *J. Chem. Educ.* **2016**, *93*, 1277−1281.

(16) Ghosh, S.; Krishnan, A.; Das, P. K.; Ramakrishnan, S. Determination of Critical Micelle Concentration by Hyper-Rayleigh Scattering. *J. Am. Chem. Soc.* **2003**, *125*, 1602−1606.

(17) Zhong, H.; Yang, L.; Zeng, G.; Brusseau, M. L.; Wang, Y.; Li, Y.; Liu, Z.; Yuan, X.; Tan, F. Aggregate-based sub-CMC solubilization of hexadecane by surfactants. *RSC Adv.* **2015**, *5*, 78142−78149.

(18) Kalyanasundaram, K.; Thomas, J. K. Environmental Effects on Vibronic Band Intensities in Pyrene Monomer Fluorescence and Their Application in Studies of Micellar Systems. *J. Am. Chem. Soc.* **1977**, *99*, 2039−2044.

(19) Vendittis, E. D.; Palumbo, G.; Parlato, G.; Bocchini, V. A Fluorimetric Method for the Estimation of the Critical Micelle Concentration of Surfactants. *Anal. Biochem.* **1981**, *115* (2), 278−286.

(20) Piñeiro, L.; Novo, M.; Al-Soufi, W. Fluorescence emission of pyrene in surfactant solutions. *Adv. Colloid Interface Sci.* **2015**, *215*, 1−12.

(21) Kurniasih, I. N.; Liang, H.; Mohr, P. C.; Khot, G.; Rabe, J. P.; Mohr, A. Nile Red Dye in Aqueous Surfactant and Micellar Solution. *Langmuir* **2015**, *31*, 2639−2648.

(22) Kumbhakar, M.; Nath, S.; Mukherjee, T.; Pal, H. Solvation dynamics in triton-X-100 and triton-X-165 micelles: Effect of micellar size and hydration. *J. Chem. Phys.* **2004**, *121*, 6026−6033.

(23) Fluksman, A.; Benny, O. A robust method for critical micelle concentration determination using coumarin-6 as a fluorescent probe. *Anal. Methods* **2019**, *11*, 3810−3818.

(24) Matsuura, K.; Hisamoto, K.; Tanaka, T.; Sakamoto, R.; Okazaki, M.; Inaba, H. Turn-On Fluorescent Probe Based on a Dansyl Triarginine Peptide for Ganglioside Imaging. *ACS Org. Inorg. Au.* **2021**, *1*, 60−67.

(25) Mei, J.; Leung, N. L. C.; Kwok, R. T. K.; Lam, J. W. Y.; Tang, B. Z. Aggregation-Induced Emission: Together We Shine, United We Soar! *Chem. Rev.* **2015**, *115*, 11718−11940.

(26) Wu, S.; Liang, F.; Hu, D.; Li, H.; Yang, W.; Zhu, Q. Determining the Critical Micelle Concentration of Surfactants by a Simple and Fast Titration Method. *Anal. Chem.* **2020**, *92*, 4259−4265.

(27) Kang, M.; Zhang, Z.; Song, N.; Li, M.; Sun, P.; Chen, X.; Wang, D.; Tang, B. Z. Aggregation-enhanced theranostics: AIE sparkles in biomedical field. *Aggregate* **2020**, *1*, 80−106.

(28) Zhao, X.; Wang, Y.; Wang, Q.; Li, Q.; Liu, Z.; Zhu, W.-H. An environmentally friendly AIE probe for CMC determination. *Mater. Chem. Front.* **2022**, *6*, 1005−1009.

(29) Wu, R.; Tian, M.; Shu, C.; Zhou, C.; Guan, W. Determination of the critical micelle concentration of surfactants using fluorescence strategies. *Soft Matter.* **2022**, *18*, 8920−8930.

(30) Mohr, A.; Talbiersky, P.; Korth, H.-G.; Sustmann, R.; Boese, R.; Bläser, D.; Rehage, H. A New Pyrene-Based Fluorescent Probe for the Determination of Critical Micelle Concentrations. *J. Phys. Chem. B* **2007**, *111*, 12985−12992.

(31) Hussain, E.; Niu, N.; Zhou, H.; Shahzad, S. A.; Yu, C. Aggregation enhanced excimer emission (AEEE) of benzo[*ghi*]-perylene and coronene: multimode probes for facile monitoring and direct visualization of micelle transition. *Analyst* **2018**, *143*, 4283−4289.

(32) Förster, T. Excimers. *Angew. Chem., Int. Ed.* **1969**, *8*, 333−343.

(33) Bains, G. K.; Kim, S. H.; Sorin, E. J.; Narayanaswami, V. The Extent of Pyrene Excimer Fluorescence Emission Is a Reflector of Distance and Flexibility: Analysis of the Segment Linking the LDL Receptor-Binding and Tetramerization Domains of Apolipoprotein E3. *Biochemistry* **2012**, *51*, 6207−6219.

(34) Kim, S. K.; Lee, S. H.; Lee, J. Y.; Lee, J. Y.; Bartsch, R. A.; Kim, J. S. An Excimer-Based, Binuclear, On−Off Switchable Calix[4]crown Chemosensor. *J. Am. Chem. Soc.* **2004**, *126* (50), 16499−16506.

(35) Kim, H. J.; Hong, J.; Hong, A.; Ham, S.; Lee, J. H.; Kim, J. S. Cu^{2+}-Induced Intermolecular Static Excimer Formation of Pyrenealkylamine. *Org. Lett.* **2008**, *10*, 1963−1966.
(36) Jung, H. S.; Park, M.; Han, D. Y.; Kim, E.; Lee, C.; Ham, S.; Kim, J. S. Cu^{2+} Ion-Induced Self-Assembly of Pyrenylquinoline with a Pyrenyl Excimer Formation. *Org. Lett.* **2009**, *11*, 3378−3381.
(37) Nishizawa, S.; Kato, Y.; Teramae, N. Fluorescence Sensing of Anions via Intramolecular Excimer Formation in a Pyrophosphate-Induced Self-Assembly of a Pyrene-Functionalized Guanidinium Receptor. *J. Am. Chem. Soc.* **1999**, *121*, 9463−9464.
(38) Rhee, H.-W.; Lee, C.-R.; Cho, S.-H.; Song, M.-R.; Cashel, M.; Choy, H. E.; Seok, Y.-J.; Hong, J.-I. Selective Fluorescent Chemosensor for the Bacterial Alarmone (p)ppGpp. *J. Am. Chem. Soc.* **2008**, *130*, 784−785.
(39) Xu, Z.; Singh, N. J.; Lim, J.; Pan, J.; Kim, H. N.; Park, S.; Kim, K. S.; Yoon, J. Unique Sandwich Stacking of Pyrene-Adenine-Pyrene for Selective and Ratiometric Fluorescent Sensing of ATP at Physiological pH. *J. Am. Chem. Soc.* **2009**, *131*, 15528−15533.
(40) Dai, Q.; Liu, W.; Zhuang, X.; Wu, J.; Zhang, H.; Wang, P. Ratiometric Fluorescence Sensor Based on a Pyrene Derivative and Quantification Detection of Heparin in Aqueous Solution and Serum. *Anal. Chem.* **2011**, *83*, 6559−6564.
(41) Zhang, R.; Tang, D.; Lu, P.; Yang, X.; Liao, D.; Zhang, Y.; Zhang, M.; Yu, C.; Yam, V. W. W. Nucleic Acid-Induced Aggregation and Pyrene Excimer Formation. *Org. Lett.* **2009**, *11*, 4302−4305.
(42) Wu, J.; Zou, Y.; Li, C.; Sicking, W.; Piantanida, I.; Yi, T.; Schmuck, C. A Molecular Peptide Beacon for the Ratiometric Sensing of Nucleic Acids. *J. Am. Chem. Soc.* **2012**, *134*, 1958−1961.
(43) Chen, J.; Liao, D.; Wang, Y.; Zhou, H.; Li, W.; Yu, C. Real-Time Fluorometric Assay for Acetylcholinesterase Activity and Inhibitor Screening through the Pyrene Probe Monomer−Excimer Transition. *Org. Lett.* **2013**, *15*, 2132−2135.
(44) Xie, H.; Jiang, X.; Zeng, F.; Yu, C.; Wu, S. A novel ratiometric fluorescent probe through aggregation-induced emission and analyte-induced excimer dissociation. *Sens. Actuators, B* **2014**, *203*, 504−510.
(45) Qiao, M.; Fan, J.; Ding, L.; Fang, Y. Fluorescent Ensemble Sensors and Arrays Based on Surfactant Aggregates Encapsulating Pyrene-Derived Fluorophores for Differentiation Applications. *ACS Appl. Mater. Interfaces* **2021**, *13*, 18395−18412.
(46) Pacheco-Liñán, P. J.; Alonso-Moreno, C.; Ocaña, A.; Ripoll, C.; García-Gil, E.; Garzón-Ruíz, A.; Herrera-Ochoa, D.; Blas-Gómez, S.; Cohen, B.; Bravo, I. Formation of Highly Emissive Anthracene Excimers for Aggregation-Induced Emission/Self-Assembly Directed (Bio)imaging. *ACS Appl. Mater. Interfaces* **2023**, *15*, 44786−44795.
(47) Nakahara, Y.; Kida, T.; Nakatsuji, Y.; Akashi, M. New Fluorescence Method for the Determination of the Critical Micelle Concentration by Photosensitive Monoazacryptand Derivatives. *Langmuir* **2005**, *21*, 6688−6695.
(48) Zhu, G.; Zhang, L.; Wang, Y.; Xu, X.; Peng, X. Interactions between pyrene and pyridinium ionic liquids studied by ultraviolet−visible spectroscopy. *J. Mol. Liq.* **2016**, *213*, 289−293.
(49) Siu, H.; Duhamel, J. Molar Absorption Coefficient of Pyrene Aggregates in Water. *J. Phys. Chem. B* **2008**, *112*, 15301−15312.
(50) Zhao, L.; Ren, X.; Yan, X. Assembly Induced Super-Large Red-Shifted Absorption: The Burgeoning Field of Organic Near-Infrared Materials. *CCS Chem.* **2021**, *3*, 678−693.
(51) Bahri, M. A.; Hoebeke, M.; Grammenos, A.; Delanaye, L.; Vandewalle, N.; Seret, A. Investigation of SDS, DTAB and CTAB micelle microviscosities by electron spin resonance. *Colloids Surf., A* **2006**, *290*, 206−212.
(52) Schürholz, T.; Kehne, J.; Gieselmann, A.; Neumann, E. Functional Reconstitution of the Nicotinic Acetylcholine Receptor by CHAPS Dialysis Depends on the Concentrations of Salt, Lipid, and Protein. *Biochemistry* **1992**, *31*, 5067−5077.
(53) Chatterjee, A.; Moulik, S. P.; Sanyal, S. K.; Mishra, B. K.; Puri, P. M. Thermodynamics of Micelle Formation of Ionic Surfactants: A Critical Assessment for Sodium Dodecyl Sulfate, Cetyl Pyridinium Chloride and Dioctyl Sulfosuccinate (Na Salt). by Microcalorimetric, Conductometric, and Tensiometric Measurements. *J. Phys. Chem. B* **2001**, *105*, 12823−12831.
(54) Naskar, B.; Dey, A.; Moulik, S. P. Counter-ion Effect on Micellization of Ionic Surfactants: A Comprehensive Understanding with Two Representatives, Sodium Dodecyl Sulfate (SDS). and Dodecyltrimethylammonium Bromide (DTAB). *J. Surfactants Deterg.* **2013**, *16*, 785−794.
(55) Paula, S.; Süs, W.; Tuchtenhagen, J.; Blume, A. Thermodynamics of Micelle Formation as a Function of Temperature: A High Sensitivity Titration Calorimetry Study. *J. Phys. Chem.* **1995**, *99*, 11742−11751.
(56) Baek, K.; Eom, M. S.; Kim, S.; Han, M. S. Metal ion-prompted pyrene−excimer formation via an anion-mediated process and its application for a ratiometric Zn^{2+} chemosensor with high selectivity over Cd^{2+}. *Tetrahedron Lett.* **2013**, *54*, 1654−1657.
(57) Cabral, A. D.; Murcar-Evans, B. I.; Toutah, K.; Bancerz, M.; Rosa, D.; Yuen, K.; Radu, T. B.; Ali, M.; Penkul, A.; Kraskouskaya, D.; Gunning, P. T. Structure−activity relationship study of ProxyPhos chemosensors for the detection of proximal phosphorylation and other phosphate species. *Analyst* **2017**, *142*, 3922−3933.
(58) Kim, J.; Oh, J.; Han, M. S. Versatile small molecule kinase assay through real-time, ratiometric fluorescence changes based on a pyrene-DPA-Zn^{2+} complex. *RSC Adv.* **2021**, *11*, 10375−10380.
(59) Kim, J.; Oh, J.; Han, M. S. A ratiometric fluorescence probe for the selective detection of H_2S in serum using a pyrene-DPA−Cd^{2+} complex. *RSC Adv.* **2021**, *11*, 24410−24415.

https://doi.org/10.1021/acsomega.5c08403
ACS Omega 2025, 10, 56431−56438